

Full length article

Element-specific amorphization of vacancy-ordered GeSbTe for ternary-state phase change memory

Xue-Peng Wang ^a, Xian-Bin Li ^{a,c,*}, Nian-Ke Chen ^a, Qi-Dai Chen ^a, Xiao-Dong Han ^b, Shengbai Zhang ^{a,c}, Hong-Bo Sun ^a

^a State Key Laboratory on Integrated Optoelectronics, College of Electronic Science and Engineering, Jilin University, Changchun, 130012, China

^b Beijing Key Laboratory and Institute of Microstructure and Property of Advanced Materials, Beijing University of Technology, Beijing, 100124, China

^c Department of Physics, Applied Physics and Astronomy, Rensselaer Polytechnic Institute, Troy, NY, 12180, USA

ARTICLE INFO

Article history:

Received 28 February 2017

Received in revised form

2 July 2017

Accepted 3 July 2017

Available online 4 July 2017

Keywords:

First-principles calculations

Molecular dynamics simulations

Phase transition

Electronic structure

Ternary-state memory

ABSTRACT

GeSbTe alloys have the ability of rapidly transforming between amorphous and crystalline phases. Therefore, they can be used in the non-volatile phase change memory. Recently, a vacancy-ordered cubic $\text{Ge}_2\text{Sb}_2\text{Te}_5$ (VOC GST) phase change material where the vacancies are highly ordered in the (111) plane, has been experimentally demonstrated by STEM. However, studies are mainly on the structural characterization, rather than on the phase change behavior and possible applications of the VOC GST. Here, using first-principles molecular dynamic simulations, we study the melt-quenched amorphization process and its possible applications. We find that the VOC GST exhibits a quasi-two-dimensional amorphization process that is triggered by the diffusion of Ge atoms but not others. A partial amorphous (*P-amor*) phase is obtained, which can act as an intermediate state between the pure amorphous and pure crystalline phases for possible ternary-state data storage.

© 2017 Acta Materialia Inc. Published by Elsevier Ltd. All rights reserved.

1. Introduction

Phase change materials are a class of chalcogenides which can be used for optical and electrical data storage in non-volatile phase change memory. Phase change materials have the ability of rapidly transforming between amorphous and crystalline phases [1]. There are significant contrasts of electrical and optical properties, such as electrical resistivity and reflectivity, between the two phases [2]. This phase transition can be induced by a high temperature, a laser or an electrical pulse [3]. Among chalcogenides, $\text{Ge}_2\text{Sb}_2\text{Te}_5$ (GST) [4] is known to be the most widely studied phase change material. It exhibits many excellent phase-transition properties, for example, rapid switching rate, good data retention, and high cycling times (10^{11} in Sb-rich GST [5]). Many efforts have been made to explore the structure [6–8], switching mechanism [9,10], as well as novel applications [11] for the GST and other phase change materials.

GST has at least two crystalline phases, one is the metastable cubic phase and the other is the stable hexagonal phase. Generally

speaking, the cubic (or rock-salt) phase can be obtained by heating an amorphous sample above the crystallization temperature of about 150 °C [12]. The hexagonal phase is obtained if continuing heating up to about 300 °C [12]. Cubic GST has a NaCl type ($Fm\bar{3}m$) lattice [13], but GST is proposed to be resonant bonded material [14]. In cubic GST, the anion-like sites are occupied by Te, while the cation-like sites are occupied by Ge, Sb, and 20% cation-like vacancies, respectively. It has been pointed out that these vacancies play a crucial role both in the structure evolution and in the change of the physical properties, such as the metal-insulator transition [15,16]. Beside, more vacancy layers will reduce lattice thermal conductivity, thereby increasing thermoelectric figure of merit (ZT) in GeTe-rich GST. That results in the controlling of the thermoelectric characteristics [17].

According to the X-ray diffraction data [18] and STEM -EDX measurements [19], the vacancies have a random distribution. However, theory suggests a clustering of the vacancies to lower their energy [20,21]. By using the spherical aberration-aberration corrected high angle annular dark fields scanning transmission electron microscopy (HAADF-STEM), we recently observed a new cubic GST phase in which the vacancies are highly ordered in the (111) planes [22]. This vacancy ordered cubic (VOC) GST phase can be obtained by annealing amorphous samples at 300 °C for 10 min.

* Corresponding author. State Key Laboratory on Integrated Optoelectronics, College of Electronic Science and Engineering, Jilin University, 2699 Qianjin Street, Changchun, 130012, China.

E-mail address: lixianbin@jlu.edu.cn (X.-B. Li).

Therefore, GST has at least three crystalline phases: two cubic phases (vacancy random and vacancy ordered) and one hexagonal phase. This vacancy-ordered phase has also been observed by Bragaglia et al. [23] and Ross et al. [24]. Moreover, the vacancy layers could disappear, reappear, and move under scanning of the electron beam [25].

Since our work on VOC GST, we notice that the vacancy ordering phenomena has previously been observed in bulk GeTe-rich GST by Oeckler et al. [26–28]. Because the hexagonal phase can be viewed as having vacancies concentrated on the cation-like layers (i.e. forming van der Waals gap between adjacent Te layers), the VOC phase may be considered as an intermediate structure between the random vacancy cubic and hexagonal phases [29]. Moreover, our first-principles molecular dynamic simulations reveal that melting is initiated around the vacancy layers of VOC GST, which propagate to nearby regions [22]. Hence, it is possible to control the phase change behavior of VOC GST by different experimental conditions, for example, having a different duration of the pulse. Currently, studies are mainly on the structural characterization, rather than on the dynamic behavior and possible applications of the new VOC phase.

In recent years, phase change materials have drawn attentions from new applications such as brain-inspired/neuromorphic computing, and ternary content addressable memory [30]. In the latter case, besides the two states of “0” and “1”, there is a third state of wildcard (don’t care), which may be used for ultrafast fuzzy query [31]. Based on the discussion above, ternary- or even multiinary phase changes can be realized by controlling the intermediate phases, for example, in the intermediate state of $\text{Ga}_2\text{Te}_3\text{Sb}_5$, only the regions near grain boundaries become disordered [32]. Due to the different crystallization temperatures between GeTe and Sb_2Te_3 , a GeTe-Sb₂Te₃ superlattice-like structure also exhibits three states: namely, entirely amorphous, amorphous GeTe plus crystalline Sb₂Te₃, and entirely crystalline phases [33]. For neuromorphic computing, on the other hand, the device should have different responses under different input signals, which can be realized by multi-level states. To date, eight-level data storage and three-bits in a single cell based on GST has been reported [34]. By a molecular dynamic simulation, Skelton et al. found stepwise changes in the structural order of GST in response to temperature pulses with a varying length and duration [35].

In this work, we study the RESET (amorphization) process of VOC GST, by which we propose a scheme to realize a ternary state. First-principles molecular dynamics shows that the final RESET structures are determined by the melting time (which mimics the pulse duration in actual devices). At the initial stage of melting of the VOC phase, Ge penetrates through Te layers to the vacancy-ordered layers. It also means a vacancy diffusion. When the time is short, we obtain a partial amorphous (*P-amor*) phase. Only regions near the vacancy layers can melt and change to amorphous phase where Sb and Te still hold a defective octahedral *p*-bonding network. As such, only 22.2% Ge exhibits the tetrahedral *sp*³ bonding, which is considerably less than that in a standard amorphous phase. The calculated imaginary part of permittivity (ϵ_2) indicates that the *P-amor* phase is intermediate between pure crystalline and amorphous phases, as required for ternary-state data storage.

2. Simulation methods

Our calculation employs density functional theory (DFT) [36], as implemented in the Vienna *ab initio* simulation package (VASP) codes [37]. The projector augmented wave (PAW) pseudopotentials [38] are used for electron-ion interaction, whereas the electron exchange-correlation interaction is described by the Perdew-

Burke-Ernzerhof (PBE) functional [39]. We use the *NVT* canonical ensemble for *ab initio* molecular dynamic (MD) simulations, in which the Nosé thermostat is used to control the temperature [40]. In the MD, the energy cutoff is 200 eV, the time step is 3 fs, the Gaussian smearing is 0.1 eV, a single K-point is used, and no spin is considered. Our structural model is built based on a NaCl type rock-salt GST supercell. The lattice parameters ($a = b = c = 12.0292 \text{ \AA}$) of the initial cell are set to match the density measured by experiment (6.27 g/cm^3) [41]. To study vacancy redistribution, we redefine a new lattice vectors of $(1\ 1\ 1)$, $(-1\ -1\ 0)$, and $(-1\ -1\ -2)$ in terms of the initial rock-salt supercell as principal axes. The redefined lattice contains 172 atoms ($\text{Ge}_{38}\text{Sb}_{38}\text{Te}_{96}$) and 20 vacancies. In the redefined lattice, 16 cation-like sites in a $(1\ 1\ 1)$ layer are fully occupied by vacancies while other cation-like sites are randomly occupied by Ge, Sb, or the other 4 vacancies. In this way, we build a VOC GST calculation model. After optimization, the density of calculation model decreases to 6.02 g/cm^3 in calculation. The lattice parameters of the optimized cell are $a = 21.39580 \text{ \AA}$, $b = 17.17649 \text{ \AA}$, $c = 14.80514 \text{ \AA}$, $\alpha = 89.98^\circ$, $\beta = 90.70^\circ$, $\gamma = 90.01^\circ$. For more details of modeling process, see Part 1 of the supporting information (SI). Finally, the MD simulation is carried out from the optimized model. As shown in Fig. 1, RESET process is achieved by the melt-quenched method where melting is performed at 1300 K for 6ps and 9ps, respectively, followed by two rapid quenching processes to 300 K. Then the samples are maintained for another 39ps at 300 K. Here, the high melting temperature of 1300 K (compared to the melting point of 900 K) is used to accelerate melting, and the quenching rate also has little effect on our results, see Part 2 and 3 of the SI. We used the last 1000 steps (36ps–39ps) in equilibrium state (see Part 4 of the SI) to analyze the atomic structure, such as distributions of bond angle and *local order parameter* [42]. The results are averaged in the 1000 steps. The sum of $1.2 \times$ the covalent radius is used as the bond length cutoff for every two atoms.

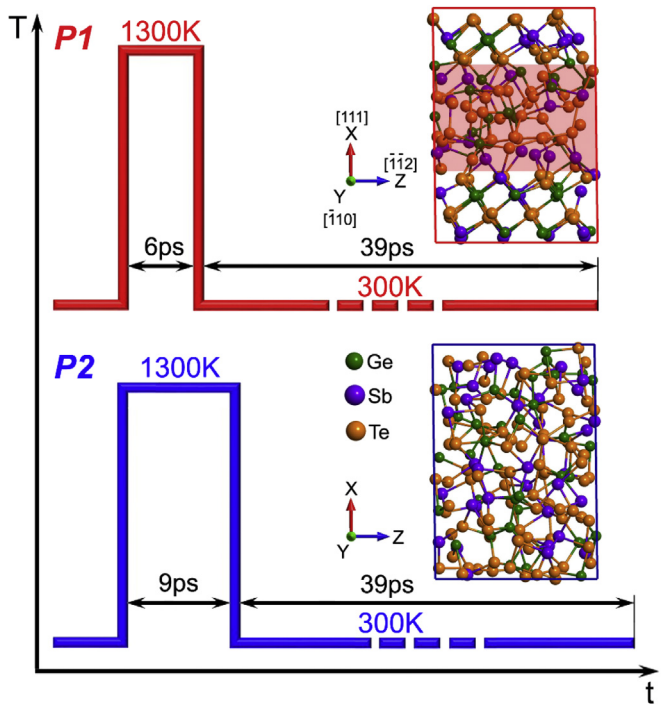


Fig. 1. Temperature evolution during two melt-quenched RESET processes (P1, P2) in VOC GST and final RESET structures. Region shadowed by red in P1 final RESET structure is the amorphous part of the *P-amor* phase. Atoms color coding: Green for Ge, purple for Sb and orange for Te. (For interpretation of the references to colour in this figure legend, the reader is referred to the web version of this article.)

3. Results and discussion

Fig. 1 displays the temperature evolution and the final RESET structures of the two melt-quenched processes. As pointed out in our previous work [22], the melting starts around the vacancy layer of the VOC phase. By applying a short RESET pulse, which corresponds to 1300 K melting for 6ps followed by a room-temperature quenching in our simulation, we can get a *P-amor* phase where only the regions around the vacancy layer transform into amorphous states, see the final RESET structure of the P1 process in **Fig. 1**. This indicates a quasi-two-dimensional RESET process. If we use a longer RESET pulse, for instance, 1300 K melting for 9ps in our simulation, all the atoms diffuse randomly and leads to a pure amorphous phase, see the final RESET structure of the P2 process.

To find out the driving force in the RESET process, **Fig. 2** shows the key snapshots at the beginning of the melting (2–4ps) when Ge (but not Sb) firstly diffuses into the vacancy layer. We highlight the Ge and Te atoms related to the diffusion. **Fig. 2(a)** shows the VOC phase is still periodic at 2.25ps. Two Ge (*i.e.* Ge1 and Ge2 closing vacancy layer) stay in their original octahedral position. At 2.7 ps [**Fig. 2(b)**], the Ge1 gets to the vacancy layer by diffusing through a Te layer and bonds with the atom in another Te layer, which is also found in the trace of coordinates along the X-direction ([111] in the VOC phase) during the melting in **Fig. 2(e)**. In this way, Ge1 forms a tetrahedral-bonding configuration in the vacancy layer, see the bond angle distribution in **Fig. S5** of the SI. It should be pointed out that the tetrahedral configuration is just a transient state. While, Sb

and Te keep the layered trajectory in the initial stage of melting. The trace of coordinates of all the atoms during the whole melt-quenched process are given in **Fig. S6** of the SI. When the time goes to 3.12 ps [**Fig. 2(c)**], the Ge2 also passes through another Te layer next to the vacancy layer. At 3.39ps [**Fig. 2(d)**], the Ge1 has changed to an octahedral configuration. As the Ge1 does, the Ge2 also enters into the vacancy layer, forms the transient tetrahedral-bonding configuration, and then changes to the octahedral configuration. It can be further confirmed by a bond angle distribution (melting time between 4.5ps and 6ps) of the Ge atoms that have entered into the vacancy layer and other Ge atoms. As shown in **Fig. 2(f)**, they have almost the same bond angle distributions which are peaked at 90°. As a result, lack of atoms in cation-like layer that next to the vacancy layer and a random occupation of Ge in vacancy layer trigger an amorphization instantly in the area around the vacancy layer and lead to the *P-amor* phase, see the further proofs in Part 7 of the SI. In contrast, Sb has a robust *p*-bonding with Te [43]. Thus, its bonding network is difficult to be changed frequently as Ge does. This is a reason why only Ge but not Sb trigger the RESET process in VOC phases.

Next, the structure of the *P-amor* phase is investigated. First, the amorphous part of the *P-amor* phase has the atoms with the X-direction coordinates between 0.3 and 0.75 (region shadowed by red color in **Fig. 1**). According to the bond angle distribution here (**Fig. S6** in the SI), Sb and Te hold the octahedral *p*-bonding configuration while some Ge exhibit *sp*³ bonding characteristics. This is not surprised due to many experiments finding *sp*³ Ge in

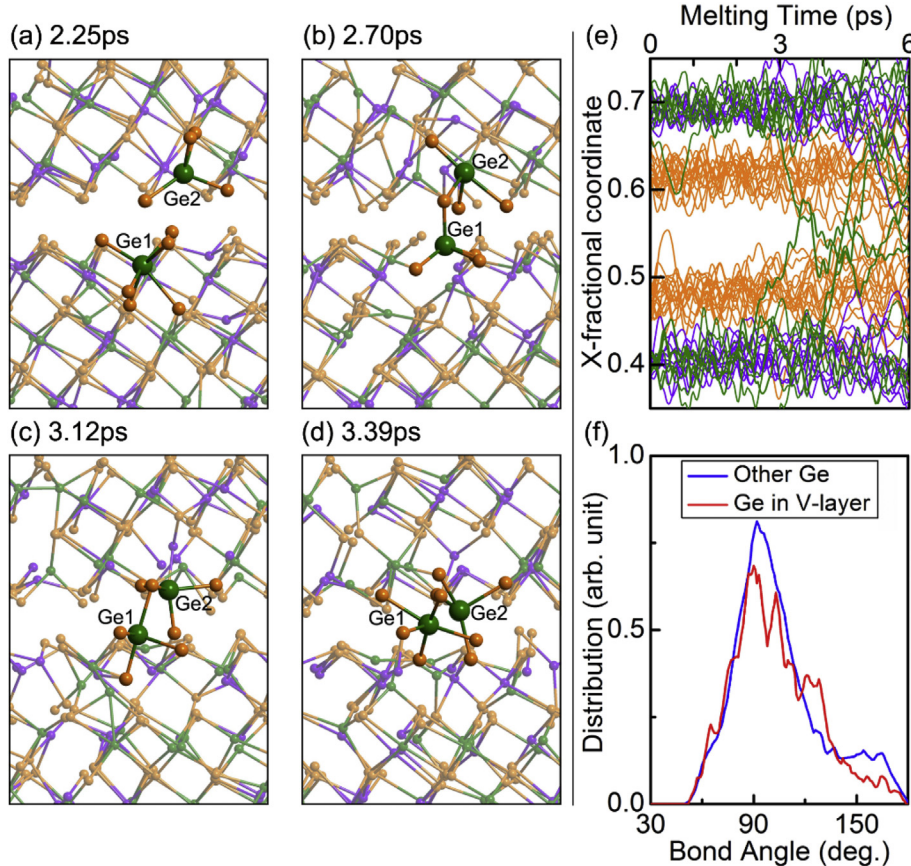


Fig. 2. Key snapshots of Ge at different melting times: (a) 2.25ps, (b) 2.7ps, (c) 3.12ps, and (d) 3.39ps, which trigger the RESET process in VOC GST. Two Ge atoms (Ge1 and Ge2 that diffuse into the vacancy-ordered layer) and the surrounding Te atoms are highlighted. Atoms color code is the same as in **Fig. 1**. (e) X-fractional coordinates of Ge (green), Sb (purple), and Te (orange) during melting process. The coordinates between 0.5 and 0.6 refer to the original vacancy layer. (f) The average bond angle distribution (melting time between 4.5ps and 6ps) of Ge atoms that have entered into the vacancy layer (red line) and the other Ge (blue line), respectively. (For interpretation of the references to colour in this figure legend, the reader is referred to the web version of this article.)

amorphous GST [44,45]. Here, we use the *local order parameter* (q) to compare bonding environments of Ge in both the pure amorphous phase and the amorphous part of the *P-amor* phase. q is defined as $q = 1 - \frac{3}{8} \sum_{i>k} \left(\frac{1}{3} + \cos \theta_{ijk} \right)^2$, $0 < \theta \leq 180^\circ$, where the sum of the bond angle runs over couples of atoms bonded to a central atom j [42,46]. This parameter is used to identify the contents of local octahedral and tetrahedral bonding configurations for a specific element. Fig. 3(a) shows the q distributions for the four-coordinated Ge have two peaks: one at 0.7 and the other at 0.9 that are corresponding to the defective octahedral and the tetrahedral configurations, respectively [42,46]. The distributing intensity peaked at 0.9 is significantly small in amorphous part of the *P-amor* phase. By integrating q -distribution in the range closing to 0.9 (0.8–1.0, dark gray area in Fig. 3), 33.8% of Ge atoms are found to have the tetrahedral configuration in pure amorphous phase, which agrees with the work by Caravati et al. [42]. In contrast, only 22.2% of Ge atoms are found to hold the tetrahedral configuration in amorphous part of the *P-amor* phase. The reduction of tetrahedral Ge here is due to the proximity effect [47]

of the two rock-salt crystalline templates that sandwich the amorphous part. Besides, there are much fewer homopolar bonds (Ge-Ge and Ge-Sb) in the *P-amor* phase than pure amorphous phase, see Part 9 of the SI. This may be the other reason that lead to reduction of tetrahedral Ge. Because homopolar bonds can significantly stabilize the tetrahedral units [48,49]. Fig. 3(b) shows the voids in pure amorphous phase are uniform and small while in the *P-amor* phase the voids are larger and mainly in the amorphous part. Here, with enough space for atomic rearrangement [50,51], these voids are favorable for crystallization in the *P-amor* phase, i.e. SET process in memory. In order to study the stability of the *P-amor* phase, the sample is further annealed for another 300ps at 300 K. As shown in Fig. 3(b), the amorphous part with large voids can be maintained even after the long-period annealing. According to the *local order parameter* distribution of the amorphous part of the *P-amor* phase that annealing for 300ps, the proportion of Ge that hold tetrahedral configuration just slightly decreases from the original 22.2% to 19.3%, see Fig. 3(a). Furthermore, the two peaks corresponding to octahedral (around 0.7) and tetrahedral (close to 1) configurations become more

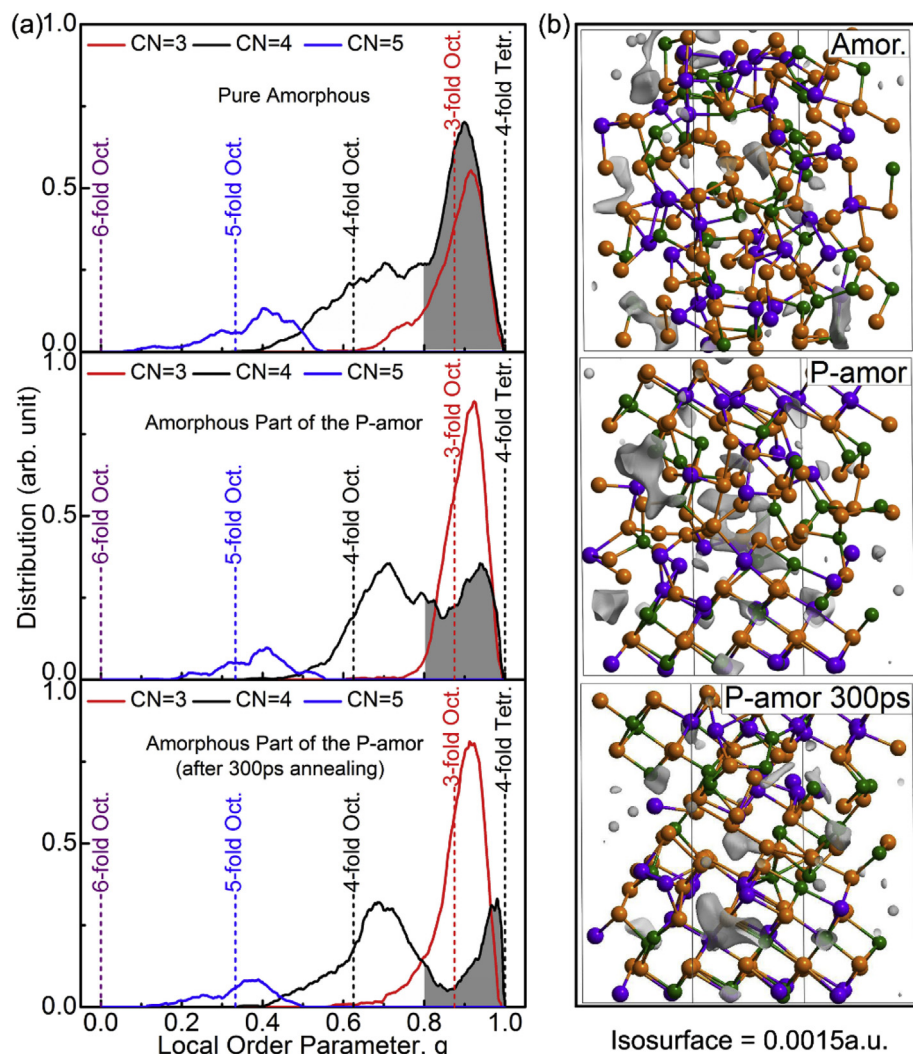


Fig. 3. Bonding geometries and void distributions of pure amorphous phase (Amor), amorphous part of the *P-amor* phase, and amorphous part of the *P-amor* phase that further annealing for 300ps at 300 K (*P-amor* 300ps). (a) Local order parameter (q) of Ge at different coordination numbers. Vertical dash lines indicate q in the standard octahedral (Oct) and tetrahedral (Tetr) bonding environments. Regions shadowed by dark gray are closely related to tetrahedral bonding. (b) Spatial distributions of the voids (as reflected by a low density isosurface of 0.0015 a.u. in the charge density plot, grey regions) in the three phases. Atoms color code is the same as in Fig. 1. (For interpretation of the references to colour in this figure legend, the reader is referred to the web version of this article.)

clearly separated. The Ge atoms with sp^3 tetrahedral bonding topology ensure the stability of the amorphous part.

Fig. 4(a) displays the localized-electron states of the *P-amor* phase and the *P-amor* phase that further annealing for 300ps by an electron localization function (ELF) [52] with a high isosurface value (0.92). In both cases, these highly localized electrons (*cap-like* shape) are in form of lone pairs and only exist in the amorphous part. Therefore, there are no partial occupied dangling bonds here. All the dangling bonds form double occupied lone pairs instead, which reduce energy and open gaps, see **Fig. 4(b)**. It is known that crystalline GST has a delocalized resonant *p*-bonding network [14] in which atoms have a coordination number of 6 and a bond angle of 90° . Due to the voids, the amorphous part of the *P-amor* phase has fewer atomic neighbors and breaks the resonant-bonding rule. As a result, the *P-amor* phase has a unique combination of the localized and delocalized electrons that are spatially separated. That makes it as an intermediate state between the pure amorphous phase and the pure crystalline phases in term of optical or electrical properties. For example, the *P-amor* phase should have a higher resistance than that of the pure crystalline phase but hold a lower resistance than that of the pure amorphous phase. **Fig. 4(c)** shows that the ε_2 in the *P-amor* phase indeed locates between those of the pure amorphous and crystalline phases. Meanwhile, this feature can be retained after the further 300ps annealing simulation. In fact, even after 600ps annealing at 300 K, the *P-amor* phase also exhibits good data retention ability, see Part 10 of the *SI*. Therefore, it indicates a potential ternary-state phase change memory.

Finally, **Fig. 5** proposes a switching scheme of the ternary-state memory based on the VOC GST. In phase change memory device,

voltage or laser pulse is used to induce phase transition. Generally, to obtain amorphous phase from crystalline phase (RESET) in a typical binary memory, a short duration pulse with high amplitude (red pulse t_{CA} in **Fig. 5**) is applied. The strong Joule heat will sufficiently melt the material which is then rapidly quenched into the amorphous phase. To recrystallize from the amorphous phase (SET), a long pulse with low amplitude (blue pulse t_{CP}) is applied to raise the temperature over its glass transition temperature but lower than its melting point. The melting process of the VOC GST can be more easily controlled than that of the typical vacancy-random cubic GST [22]. As mentioned above, the *P-amor* phase can be easily created from the VOC phase by an appropriate melting time, i.e. an appropriate duration of the RESET pulse. Therefore, we propose to apply a RESET pulse with high amplitude to melt the VOC phase. But the duration should be shorter [$t_{CP}(\text{RESET}) < t_{CA}(\text{RESET})$] in order to prevent complete amorphization and obtain the *P-amor* phase. If another pulse with high amplitude [$t_{AP}(\text{RESET})$] is applied, the *P-amor* phase will be completely disordered and transform into the pure amorphous phase. It is easier for the *P-amor* phase to transform back to the VOC phase since it has not only crystalline templates but also voids to facilitate atomic rearrangement in amorphous area [$t_{CP}(\text{SET}) < t_{CA}(\text{SET})$], see the crystallization process in Part 11 of the *SI*. However, there are still some problems in this scheme. It will take longer time to switch the pure amorphous phase into the VOC phase due to a vacancy-ordering process. On the other hand, to obtain the *P-amor* phase directly from amorphous phase is difficult. Further theoretical studies as well as more experiments are required to solve these problems. Nevertheless, there is a more practical proposal on the device of binary data storage. As only two

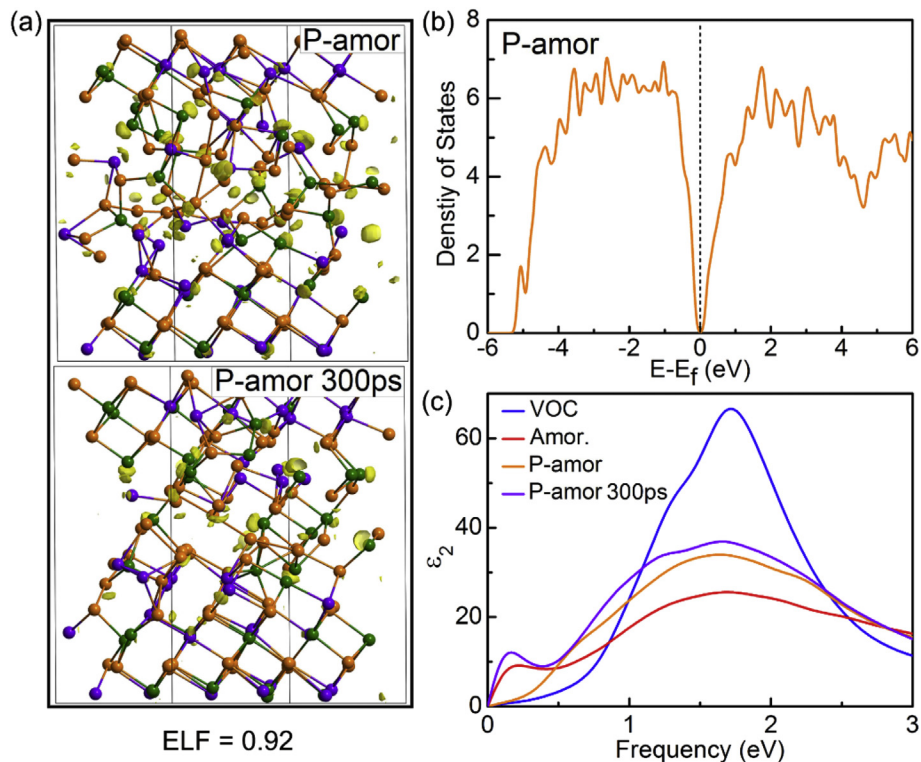


Fig. 4. Electronic properties of the *P-amor* GST. (a) Spatial distributions of highly-localized electrons (as reflected by an isosurface of ELF = 0.92, yellow dots) in the *P-amor* phase and the *P-amor* phase that further annealing for 300ps (*P-amor* 300ps). Atoms color code is the same as in **Fig. 1** (b) Density of states of the *P-amor* phase. (c) ε_2 for the VOC, the pure amorphous (Amor.), the *P-amor* phases, and the *P-amor* phase that further annealing for 300ps. (For interpretation of the references to colour in this figure legend, the reader is referred to the web version of this article.)

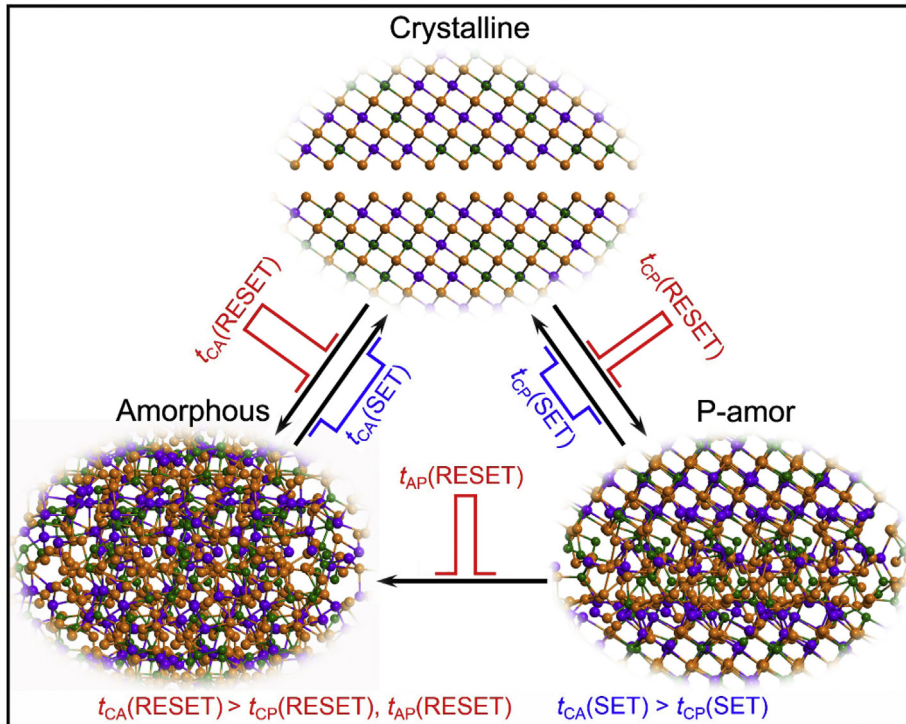


Fig. 5. Proposed switching scheme among crystalline (VOC), amorphous, and *P-amor* phases. Red pulses are required to melt the GST, while blue pulses are required to heat the GST above the glass transition temperature but below the melting point to reverse the process. t_{CA} , t_{CP} , and t_{AP} stand for the pulses used to realize crystalline-amorphous (CA) switching, crystalline-*P-amor* (CP) switching, and amorphous-*P-amor* (AP) switching, respectively. To get the *P-amor* phase, The RESET pulse t_{CP} has to be shorter than the commonly used RESET pulse t_{CA} in a typical binary memory. Atoms color code is the same as in Fig. 1. (For interpretation of the references to colour in this figure legend, the reader is referred to the web version of this article.)

logic states with distinct resistance values are required in binary data storage. The switching between the VOC and *P-amor* states could fulfill this requirement. In fact, Park et al. have obtained the VOC phase of GST in their device by an electric current [53]. So it may be possible to generate switching between the VOC and *P-amor* states in devices. Moreover, the switching between these two states could be even faster than conventional phase change memory, since only part of the phase change material needs to be switched.

4. Conclusions

In summary, a first-principles molecular dynamic simulations establishes a melt-quenched RESET picture of the VOC GST. To trigger the phase transition, Ge exchanges its position with neighboring vacancies in the vacancy-ordered layer. It results in a fast melting around the vacancy layers, whereby a quasi-two-dimensional RESET process happens. A *P-amor* phase can be obtained by using an appropriate RESET time duration. In its amorphous part, there are fewer Ge in the tetrahedral environment but larger voids, compared with a pure amorphous phase. In the *P-amor* phase, highly localized electrons stay in the amorphous region while delocalized electrons stay in the crystalline region. Therefore, its optical and electrical properties, for example, ϵ_2 , are between those of pure amorphous and crystalline phases. We also propose a feasible way to realize the ternary states among VOC, *P-amor*, and pure amorphous GST.

Acknowledgements

Work in China was supported by the NSFC (No. 11374119, No. 91423102, No. 61307119), and 973 Program (No. 2014CB921303). SBZ is supported by the U.S. DOE Office of Basic Energy Sciences

(No. DE-SC0002623). The high-performance computing center (HPCC) of Jilin University is also acknowledged for the calculation resources.

Appendix A. Supplementary data

Supplementary data related to this article can be found at <http://dx.doi.org/10.1016/j.actamat.2017.07.006>.

References

- [1] M. Wuttig, N. Yamada, Phase-change materials for rewriteable data storage, *Nat. Mater.* 6 (2007) 824–832.
- [2] S.R. Ovshinsky, Reversible electrical switching phenomena in disordered structures, *Phys. Rev. Lett.* 21 (1968) 1450–1453.
- [3] D. Lencer, M. Salinga, M. Wuttig, Design rules for phase-change materials in data storage applications, *Adv. Mater.* 23 (2011) 2030–2058.
- [4] N. Yamada, E. Ohno, K. Nishiuchi, N. Akahira, M. Takao, Rapid-phase transitions of GeTe-Sb₂Te₃ pseudobinary amorphous thin films for an optical disk memory, *J. Appl. Phys.* 69 (1991) 2849–2856.
- [5] B.K. Cheong, S. Lee, J.H. Jeong, S. Park, S. Han, Z. Wu, D.H. Ahn, Fast and scalable memory characteristics of Ge-doped SbTe phase change materials, *Phys. Status Solidi B* 249 (2012) 1985–1991.
- [6] X.Q. Liu, X.B. Li, L. Zhang, Y.Q. Cheng, Z.G. Yan, M. Xu, X.D. Han, S.B. Zhang, Z. Zhang, E. Ma, New structural picture of the Ge₂Sb₂Te₅ phase-change alloy, *Phys. Rev. Lett.* 106 (2011) 025501.
- [7] J. Akola, J. Larruea, R.O. Jones, Polymorphism in phase-change materials: melt-quenched and as-deposited amorphous structures in Ge₂Sb₂Te₅ from density functional calculations, *Phys. Rev. B* 83 (2011) 094113.
- [8] X.P. Wang, N.K. Chen, X.B. Li, Y. Cheng, X.Q. Liu, M.J. Xia, Z.T. Song, X.D. Han, S.B. Zhang, H.B. Sun, Role of the nano amorphous interface in the crystallization of Sb₂Te₃ towards non-volatile phase change memory: insights from first principles, *Phys. Chem. Chem. Phys.* 16 (2014) 10810–10815.
- [9] X.B. Li, X.Q. Liu, X. Liu, D. Han, Z. Zhang, X.D. Han, H.B. Sun, S.B. Zhang, Role of electronic excitation in the amorphization of Ge-Sb-Te alloys, *Phys. Rev. Lett.* 107 (2011) 015501.
- [10] N.K. Chen, X.B. Li, X.P. Wang, M.J. Xia, S.Y. Xie, H.Y. Wang, Z.T. Song, S.B. Zhang, H.B. Sun, Origin of high thermal stability of amorphous Ge₁Cu₂Te₃ alloy: a

- significant Cu-bonding reconfiguration modulated by Te lone-pair electrons for crystallization, *Acta Mater.* 90 (2015) 88–93.
- [11] P. Hosseini, C. David Wright, H. Bhaskaran, An optoelectronic framework enabled by low-dimensional phase-change films, *Nature* 511 (2014) 206–211.
- [12] X.L. Zhou, L.C. Wu, Z.T. Song, F. Rao, M. Zhu, C. Peng, D.N. Yao, S.N. Song, B. Liu, S.L. Feng, Carbon-doped $\text{Ge}_2\text{Sb}_2\text{Te}_5$ phase change material: a candidate for high-density phase change memory application, *Appl. Phys. Lett.* 101 (2012) 142104.
- [13] T. Nonaka, G. Ohbayashi, Y. Toriumi, Y. Mori, H. Hashimoto, Crystal structure of GeTe and $\text{Ge}_2\text{Sb}_2\text{Te}_5$ meta-stable phase, *Thin Solid Films* 370 (2000) 258–261.
- [14] K. Shportko, S. Kremers, M. Woda, D. Lencer, J. Roberson, M. Wuttig, Resonant bonding in crystalline phase-change materials, *Nat. Mater.* 7 (2008) 653–658.
- [15] W. Zhang, A. Thiess, P. Zalden, R. Zeller, P.H. Dederichs, J.-Y. Raty, M. Wuttig, S. Blügel, R. Mazzarello, Role of vacancies in metal-insulator transitions of crystalline phase-change materials, *Nat. Mater.* 11 (2012) 952–956.
- [16] T. Siegrist, P. Jost, H. Volker, M. Woda, P. Merkelbach, C. Schlockermann, M. Wuttig, Disorder-induced localization in crystalline phase-change materials, *Nat. Mater.* 10 (2011) 202–208.
- [17] T. Rosenthal, M.N. Schneider, C. Stiewe, M. Döblinger, O. Oeckler, Real structure and thermoelectric properties of GeTe-Rich germanium antimony tellurides, *Chem. Mater.* 23 (2011) 4349–4356.
- [18] N. Yamada, T. Matsunaga, Structure of laser-crystallized $\text{Ge}_2\text{Sb}_{2+x}\text{Te}_5$ sputtered thin films for use in optical memory, *J. Appl. Phys.* 88 (2000) 7020–7028.
- [19] B. Zhang, W. Zhang, Z.J. Shen, Y.J. Chen, J.X. Xue, S.B. Zhang, Z. Zhang, M. Wuttig, R. Mazzarello, E. Ma, X.D. Han, Element-resolved atomic structure imaging of rocksalt $\text{Ge}_2\text{Sb}_2\text{Te}_5$ phase-change material, *Appl. Phys. Lett.* 108 (2016) 191902.
- [20] J.L.F. Da Silva, A. Walsh, H. Lee, Insights into the structure of the stable and metastable $(\text{GeTe})_m(\text{Sb}_2\text{Te}_3)_n$ compounds, *Phys. Rev. B* 78 (2008) 224111.
- [21] Z.M. Sun, J. Zhou, R. Ahuja, Structure of phase change materials for data storage, *Phys. Rev. Lett.* 96 (2006) 055507.
- [22] B. Zhang, X.P. Wang, Z.J. Shen, X.B. Li, C.S. Wang, Y.J. Chen, J.X. Li, J.X. Zhang, Z. Zhang, S.B. Zhang, X.D. Han, Vacancy structures and melting behavior in rock-salt GeSbTe , *Sci. Rep.* 6 (2016) 25453.
- [23] V. Bragaglia, F. Arciprete, W. Zhang, A.M. Mio, E. Zallo, K. Perumal, A. Giussani, S. Cecchi, J.E. Boschker, H. Riechert, S. Privitera, E. Rimini, R. Mazzarello, R. Calarco, Metal-insulator transition driven by vacancy ordering in GeSbTe phase change materials, *Sci. Rep.* 6 (2016) 23843.
- [24] U. Ross, A. Lotnyk, E. Thelander, B. Rauschenbach, Direct imaging of crystal structure and defects in metastable $\text{Ge}_2\text{Sb}_2\text{Te}_5$ by quantitative aberration-corrected scanning transmission electron microscopy, *Appl. Phys. Lett.* 104 (2014) 121904.
- [25] A. Lotnyk, S. Bernütz, X. Sun, U. Ross, M. Ehrhardt, B. Rauschenbach, Real-space imaging of atomic arrangement and vacancy layers ordering in laser crystallised $\text{Ge}_2\text{Sb}_2\text{Te}_5$ phase change thin films, *Acta. Mater.* 105 (2016) 1–8.
- [26] M.N. Schneider, T. Rosenthal, C. Stiewe, O. Oeckler, From phase-change materials to thermoelectrics? *Z. Krist.* 225 (2010) 463–470.
- [27] P. Urban, M.N. Schneider, O. Oeckler, Temperature-dependent ordering phenomena in single crystals of germanium antimony tellurides, *J. Solid State Chem.* 227 (2015) 223–231.
- [28] M.N. Schneider, P. Urban, A. Leineweber, M. Döblinger, O. Oeckler, Influence of stress and strain on the kinetic stability and phase transitions of cubic and pseudocubic Ge-Sb-Te materials, *Phys. Rev. B* 81 (2010) 184102.
- [29] I. Hilmi, A. Lotnyk, J.W. Gerlach, P. Schumacher, B. Rauschenbach, Epitaxial formation of cubic and trigonal Ge-Sb-Te thin films with heterogeneous vacancy structures, *Mater. Des.* 115 (2017) 138–146.
- [30] C.H. Lam, Probable application for phase change memory, 15th Non-volatile Memory Technology Symposium, Beijing, China, 2015, pp. 41–42.
- [31] Q. Guo, X.C. Guo, Y.X. Bai, R.D. Patel, E. Ipek, E.G. Friedman, Resistive ternary content addressable memory systems for data-intensive computing, *IEEE Micro* 35 (2005) 62–71.
- [32] K.F. Kao, C.M. Lee, M.J. Chen, M.J. Tsai, T.S. Chin, $\text{Ga}_2\text{Te}_3\text{Sb}_5$ -a candidate for fast and ultralong retention phase-change memory, *Adv. Mater.* 21 (2009) 1695–1699.
- [33] T.C. Chong, L.P. Shi, X.Q. Wei, R. Zhao, H.K. Lee, P. Yang, A.Y. Du, Crystalline amorphous semiconductor superlattice, *Phys. Rev. Lett.* 100 (2008) 136101.
- [34] C. Rios, M. Stegmaier, P. Hosseini, D. Wang, T. Scherer, C. David Wright, H. Bhaskaran, W.H.P. Pernice, Integrated all-photonic non-volatile multi-level memory, *Nat. Phot.* 9 (2015) 725–732.
- [35] J.M. Skelton, D. Loke, T. Lee, S.R. Elliott, Ab initio molecular-dynamics simulation of neuromorphic computing in phase-change memory materials, *ACS Appl. Mater. Interfaces* 7 (2015) 14223–14230.
- [36] P. Hohenberg, W. Kohn, Inhomogeneous electron gas, *Phys. Rev.* 136 (1964) B864–B871.
- [37] G. Kresse, J. Furthmüller, Efficient iterative schemes for ab initio total-energy calculations using a plane-wave basis set, *Phys. Rev. B* 54 (1996) 11169–11186.
- [38] P.E. Blöchl, Projector augmented-wave method, *Phys. Rev. B* 50 (1994) 17953–17979.
- [39] J.P. Perdew, W. Yue, Accurate and simple density functional for the electronic exchange energy: generalized gradient approximation, *Phys. Rev. B* 33 (1986) 8800–8802.
- [40] S. Nosé, Constant temperature molecular dynamics methods, *Prog. Theor. Phys. Suppl.* 103 (1991) 1–46.
- [41] W.K. Njoroge, H.-W. Wöltgens, M. Wuttig, Density changes upon crystallization of $\text{Ge}_2\text{Sb}_{2.04}\text{Te}_{4.74}$ films, *J. Vac. Sci. Technol. A* 20 (2002) 230–233.
- [42] S. Caravati, M. Bernasconi, T.D. Kühne, M. Krack, M. Parrinello, Coexistence of tetrahedral- and octahedral-like sites in amorphous phase change materials, *Appl. Phys. Lett.* 91 (2007) 171906.
- [43] M. Luo, M. Wuttig, The dependence of crystal structure of Te-based phase-change materials on the number of valence electrons, *Adv. Mater.* 16 (2004) 439–443.
- [44] A.V. Kolobov, P. Fons, A.I. Frenkel, A.L. Ankudinov, J. Tominaga, T. Uruga, Understanding the phase-change mechanism of rewritable optical media, *Nat. Mater.* 3 (2004) 703–708.
- [45] M. Krba, A.V. Kolobov, P. Fons, J. Tominaga, S.R. Elliott, J. Hegedus, T. Uruga, Intrinsic complexity of the melt-quenched amorphous $\text{Ge}_2\text{Sb}_2\text{Te}_5$ memory alloy, *Phys. Rev. B* 83 (2011) 054203.
- [46] J.R. Errington, P.G. Debenedetti, Relationship between structural order and the anomalies of liquid water, *Nat. Lond.* 409 (2001) 318–321.
- [47] A. Ourmazd, J.C. Bean, J.C. Phillips, Submicrocrystallites and the orientational proximity effect, *Phys. Rev. Lett.* 55 (1985), 1955–1601.
- [48] V.L. Deringer, W. Zhang, M. Lumeij, S. Maintz, M. Wuttig, R. Mazzarello, R. Dronskowsk, Bonding nature of local structural motifs in amorphous GeTe , *Angew. Chem. Int. Ed. Engl.* 53 (2014) 10817–10820.
- [49] W. Zhang, V.L. Deringer, R. Dronskowsk, R. Mazzarello, E. Ma, M. Wuttig, Density-functional theory guided advances in phase-change materials and memories, *MRS Bull.* 40 (2015) 856–865.
- [50] Z.M. Sun, J. Zhou, A. Blomqvist, B. Johansson, R. Ahuja, Formation of large voids in the amorphous phase-change memory $\text{Ge}_2\text{Sb}_2\text{Te}_5$ alloy, *Phys. Rev. Lett.* 102 (2009) 075504.
- [51] T.H. Lee, S.R. Elliott, Structural role of vacancies in the phase transition of $\text{Ge}_2\text{Sb}_2\text{Te}_5$ memory materials, *Phys. Rev. B* 84 (2011) 094124.
- [52] A. Savin, O. Jepsen, J. Flad, O.K. Andersen, H. Preuss, H.G. von Schnering, Electron localization in solid-state structures of the elements: the diamond structure, *Angew. Chem. Int. Ed. Engl.* 31 (1992) 187–188.
- [53] Y.J. Park, J.Y. Cho, M.W. Jeong, S. Na, Y.C. Joo, New pathway for the formation of metallic cubic phase Ge-Sb-Te compounds induced by an electric current, *Sci. Rep.* 6 (2016) 21466.